JOURNAL OF SPACECRAFT AND ROCKETS
Vol. 45, No. 1, January–February 2008

Extension of Traditional Entry, Descent, and Landing Technologies for Human Mars Exploration

John A. Christian,* Grant Wells,† Jarret Lafleur,† Amanda Verges,‡ and Robert D. Braun§
Georgia Institute of Technology, Atlanta, Georgia 30332-0150

DOI: 10.2514/1.31929

The human exploration of Mars presents many challenges, not least of which is the task of entry, descent, and landing. Because human-class missions are expected to have landed payload masses on the order of 40 to 80 t, significant challenges arise beyond those of current robotic missions. This study uses parametric trade studies to provide insight into the feasibility of using Viking and Apollo heritage technologies to enable a human-class mission to Mars. The challenges encountered with human-class missions, as well as potential solutions, are highlighted through the results of parametric studies on vehicle size and mass. To populate the trade space, aerocapture, and entry-from-orbit analyses of 10 and 15-m diam aeroshells with a lift-to-drag ratio of 0.3 and 0.5 were investigated. The methodology developed to perform these trade studies represents a significant advancement in human Mars entry, descent, and landing system sizing. Numerous comparisons are made with past missions, both real and conceptual, and sources of discrepancies are discussed. Results indicate that in the limit, a crew capsule used only for entry from orbit could have an arrival mass as low as 20 t. For larger landed payloads, such as a 20-t surface power system, a vehicle with an arrival mass on the order of 80 t may be required. Finally, no feasible entry, descent, and landing systems were obtained with the capability to deliver more than approximately 25 t of landed payload to the Mars surface for arrival masses less than 100 t. This suggests that extension of traditional entry, descent, and landing technologies used for robotic exploration may be insufficient for human Mars exploration.

Nomenclature

A	=	aerodynamic reference area, m^2
C_D	=	drag coefficient
C_k	=	opening load factor
I_{sp}	=	specific impulse, s
L/D	=	lift-to-drag ratio
MR	=	mass ratio ($m_{arrival}/m_{final}$)
$m_{arrival}$	=	arrival mass, kg
m_{engine}	=	engine mass, kg
m_{final}	=	final mass, kg
m_m	=	parachute mortar mass, kg
m_p	=	parachute mass, kg
m_{prop}	=	propellant mass, kg
q	=	dynamic pressure, N/m^2
T	=	thrust, N
β	=	ballistic coefficient, kg/m^2
ΔV	=	change in velocity, m/s

I. Introduction

NASA'S Vision for Space Exploration [1] clearly states the agency's long-term desire to send humans to Mars. In the years since Mariner 4 became the first successful mission to reach Mars in 1965, remarkable progress has been made by robotic Mars exploration programs in the United States and abroad. To date, the United States has successfully landed five robotic spacecraft on the surface of the red planet. All of these vehicles, however, have had landed masses no greater than 600 kg [2]. In contrast, it is estimated that human missions require landed masses on the order of 40 to 80 t [3]. This will involve landing approximately 2 orders of magnitude more mass on the Martian surface in a single landing than has been achieved to date. Among the most difficult tasks in any mission to the Martian surface are entry, descent, and landing (EDL).

Through the use of parametric trade studies, this paper investigates the feasibility of human-class Mars missions by extending the EDL technologies of Viking and Apollo heritage. The trade space investigated through these studies is bounded by a number of constraints. Among the most important constraints is a deceleration limit to create an environment suitable for crewed descent, although the same vehicles can be reconfigured to deliver cargo. The exploration of the design space includes examination of a number of possible descent scenarios, sequences, and trajectories in conjunction with the required hardware. Using an Apollo-like capsule (blunt body with sidewall angle of 32 deg) and assuming a conservative atmosphere as a starting point, this study performs parametric trades on vehicle mass (20–100 t) and size (10 and 15-m diameter) for two scenarios: one with a hypersonic lift-to-drag ratio (L/D) of 0.3 and one with a hypersonic L/D of 0.5. This information is employed to size the EDL system with the objective of assessing the landed payload mass for a given Mars arrival mass and entry configuration (arrival mass is defined as the vehicle mass on the inbound hyperbolic orbit as it approaches Mars). The system-level design variables used to perform the parametric trades are summarized in Table 1.

Sizing analysis focuses on mass and volume estimation of the thermal protection system (TPS), aeroshell, parachute system, propulsion system, reaction control system, and other subsystems. This study is concluded by a thorough comparison with past missions and by placing the results in the context of previously proposed human Mars architectures. Although most estimates place the first human mission to Mars more than 25 years in the future, this investigation demonstrates the need to begin technology development today. Knowledge gained through this technology development program may be leveraged to guide the design of properly scaled robotic precursors, maximize the return from lunar exploration, and improve current human Mars mission concepts.

Presented as Paper 7427 at the Space 2006, San Jose, CA, 19–21 September 2006; received 3 May 2007; revision received 3 October 2007; accepted for publication 11 October 2007.

*Graduate Teaching Assistant, Guggenheim School of Aerospace Engineering. Student Member AIAA.
†Graduate Research Assistant, Guggenheim School of Aerospace Engineering. Student Member AIAA.
‡Undergraduate Research Scholar, Guggenheim School of Aerospace Engineering. Student Member AIAA.
§David and Andrew Lewis Associate Professor of Space Technology, Guggenheim School of Aerospace Engineering. Fellow AIAA.

Table 1 Major design space variables and ranges

Variables	Options considered
Aeroshell diameter	10 or 15 m
Vehicle mass	20–100 t
Hypersonic L/D	0.3 or 0.5
Use of supersonic parachute	Yes or no

II. Reference Mission Design

The reference mission profile investigated in this study, shown graphically in Fig. 1, begins by inserting the crewed spacecraft into orbit around Mars using aerocapture. As discussed in detail later, aerocapture is chosen for Mars capture due to the high mass fractions required for chemical propulsion. Following aerocapture, propulsive maneuvers are used to insert the vehicle into an acceptable parking orbit and then to deorbit the vehicle when it is ready to descend to the Martian surface. After a hypersonic lifting entry, the capsule continues to decelerate until the initiation of a propulsive descent phase. This powered flight phase continues until the vehicle safely touches down on the surface of Mars. The EDL systems explored within this study are designed to accommodate landing sites with surface elevations at or below 0 km MOLA (Mars orbit laser altimeter).

A. Aerocapture

To date, most robotic missions that have landed on the surface of Mars have performed a direct entry from their interplanetary transfer. A direct entry from a heliocentric arrival trajectory can have a significant mass advantage and offers operational simplicity. However, a direct entry does not offer the mission design flexibility to accommodate uncertainties in the Martian atmosphere such as dust storms. Furthermore, orbit insertion before entry reduces the peak deceleration on human crews and fits well with potential orbit rendezvous requirements for Earth return. For these reasons, this investigation assumes a human exploration architecture in which orbit insertion precedes landing. Orbit insertion around a planet with an atmosphere may be accomplished with propulsion, aerobraking, or aerocapture. Since the early 1960s, numerous studies have been performed that compare these three approaches for orbit insertion [4,5]. Aerocapture is chosen in this study.

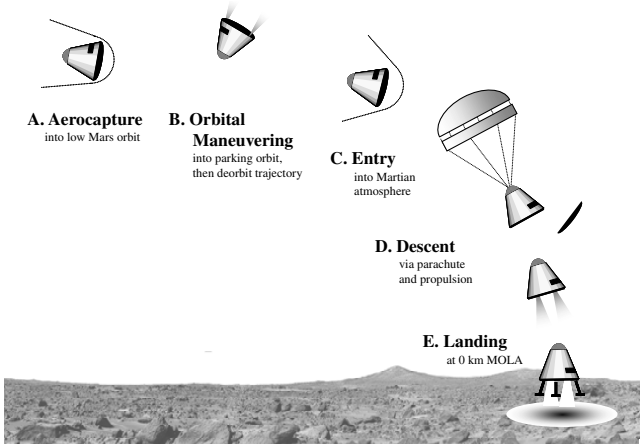

Fig. 1 Graphical depiction of baseline mission profile.

1. Limitations of Aerobraking and Propulsive Orbit Insertion

The length of time required for aerobraking (typically on the order of months) makes its use unlikely for human missions. Aerobraking for NASA's Mars Odyssey orbiter, for example, took 77 days (lasting from October 2001 through January 2002) with 332 successive drag passes to complete the aerobraking phase of the mission [6].

Although propulsive orbital insertion with traditional chemical rockets has the lowest technology development risk, it is mass prohibitive, as shown in Fig. 2 (increased mass and the resulting additional launches may make implementation of this approach more risky than other methods of orbit insertion). In interpreting the results shown in Fig. 2, recall that the propellant mass fraction is defined as $m_{\text{prop}}/m_{\text{arrival}}$. As shown in Fig. 2, arrival velocity at Mars has a large impact on propellant mass fraction, and a propellant mass fraction greater than 0.3 is required. For short duration interplanetary transfers with associated high entry velocities, a propellant mass fraction above 0.6 may be required, prohibiting this architecture selection. The choice of specific impulse (I_{sp}) and parking orbit has a moderate impact on the propellant mass fraction required, but in all cases analyzed, propulsive orbital insertion requires a significant mass fraction.

2. Advantages and Disadvantages of Aerocapture

Aerocapture has been proposed by numerous authors [2,4,5,7–10] as a means to reduce arrival mass requirements for human Mars exploration. An aerocapture maneuver slows a spacecraft from hyperbolic speed to orbital speed using a single pass through the atmosphere of a planet. As aerocapture is an unproven technique, it is important to quantify the architecture-level implications of this approach. Assuming a periapsis velocity of 6 km/s, a propulsively inserted vehicle requires a total ΔV of 2.29 km/s to complete an orbit insertion into the parking orbit used in this study (an elliptical orbit with eccentricity of 0.3 and periapsis of 3780 km) along with the subsequent deorbit maneuvers. If the required propulsive maneuvers are performed using a LOX/CH4 engine with an I_{sp} of 350 s, this ΔV translates into a mass ratio ($MR = m_{\text{arrival}}/m_{\text{final}}$) of 1.95 (equivalent to a propellant mass fraction of 0.49—see Fig. 2b). This mass fraction increases significantly with periapsis velocity (or as interplanetary transfer time is reduced).

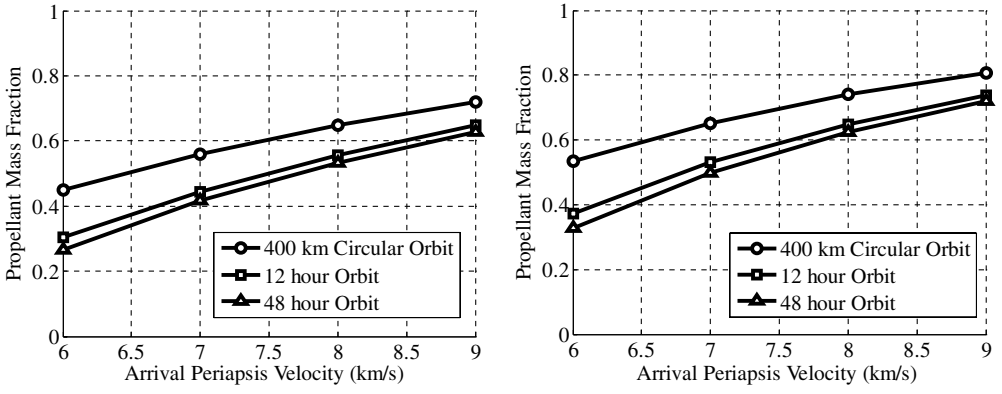

a) LOX / LH2 propellant (I_{sp} = 450 sec) **b) LOX / CH4 propellant (I_{sp} = 350 sec)**

Fig. 2 Mass fraction estimates for propulsive orbital insertion at Mars (400 km periapsis).

This analysis underscores the drastic improvement that is possible through aerocapture with a dual-use heat shield (a single heat shield that is used for both aerocapture and entry). In this case, the entry-from-orbit mass will represent a large percentage of the arrival mass. In the limit for the target orbits analyzed in this study and the dual-use heat-shield option, the entry mass may be as high as approximately 92% of the arrival mass (with the 8% primarily comprising propellant consumed for the approximately 250 m/s deorbit maneuver). Given the relatively poor performance associated with chemical propulsion for orbit insertion, the development of aerocapture technology is likely a prerequisite for human missions to Mars. Additionally, since aerocapture has not yet been flight proven, aerocapture technology is deemed a candidate for validation by precursor robotic missions. Note that high I_{sp} systems (e.g., nuclear-thermal propulsion) also provide a mass-efficient option for orbit insertion, but are not without their own technology development challenges and mission implications.

3. *Analysis of Orbit Insertion via Aerocapture*

Aerocapture trajectories are generally constrained by the three following limits, depicted in Fig. 3: 1) The lift-down trajectory allows the shallowest entry flight-path angle while meeting the exit energy constraint. This trajectory has the lowest peak heat rate and lowest peak deceleration, but the highest integrated heat load. This is also referred to as the "overshoot boundary." 2) The lift-up trajectory allows the steepest entry flight-path angle while meeting the exit energy constraint. This trajectory has the highest peak heat rate and the highest peak deceleration, but the lowest integrated heat load. This is also referred to as the "undershoot boundary." 3) The third bound is defined by the entry flight-path angle that achieves the specified peak deceleration limit with a lift-up entry (5 g in this investigation). The vehicle flies lift-up until peak deceleration, and after the limit is reached, uses bank angle modulation to achieve the desired exit energy. The 5-g limit was assumed to be the maximum tolerable deceleration for short periods by a crew of deconditioned astronauts [7,11]. For a given entry velocity, Fig. 3 defines the entry corridor performance which must be met by interplanetary navigation for a vehicle flown at an L/D of 0.3. Corridor widths on the order of 1 deg (entry velocities below about 9 km/s) are readily achievable with present technology.

An aerocapture schematic for the reference mission is provided in Fig. 4. The spacecraft enters the atmosphere with a velocity of 6 km/s, considered to be a lower velocity within a wide range of interplanetary trajectory options [8,12]. The target postaerocapture orbit for this investigation is an elliptical orbit with a semimajor axis of approximately 5212 km and an eccentricity of 0.34. Aerocapture trajectories are simulated with the program to optimize simulated trajectories (POST) [13] and flown with either an L/D of 0.3 or an L/D of 0.5. Note that the target parking orbit, as shown in Fig. 4, has a period of 3.35 h.

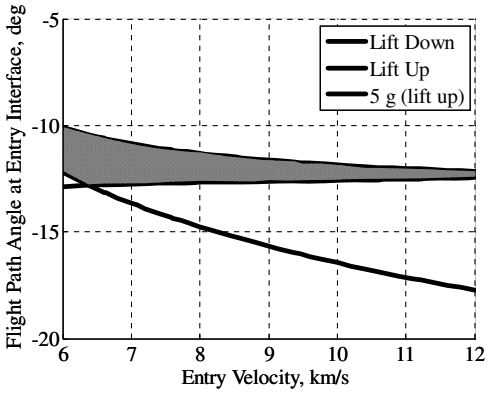

Fig. 3 An aerocapture corridor showing each boundary and the physical corridor (shaded) for $L/D = 0.3$.

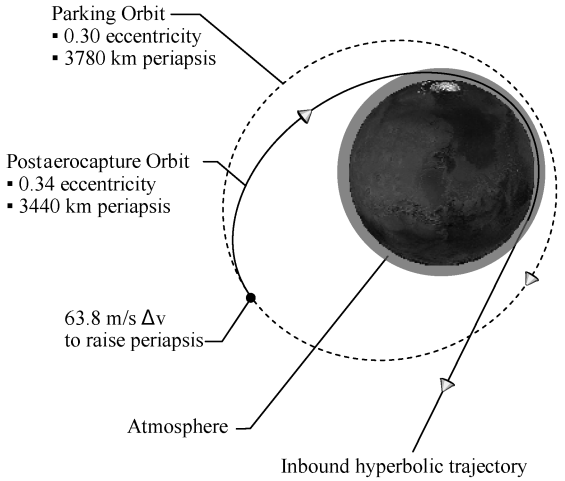

Fig. 4 Orbital maneuvers: aerocapture and insertion into parking orbit.

B. Orbital Maneuvering and Entry from Orbit

After the aerocapture maneuver, a propulsive maneuver is performed using the reaction control thrusters at apoapsis to raise periapsis and establish an elliptical parking orbit (Fig. 4). The crew remains in this orbit until they are ready to descend to the surface. Note that orbiting assets, such as the Earth return vehicle, could also be placed in this parking orbit following aerocapture. As such, the vehicle must transition to a power-safe state and establish Earth communications. From this orbit, another propulsive maneuver is used to deorbit the craft (Fig. 5) such that it meets the 4 km/s velocity and approximately −14.5 deg flight-path angle dictated by the selected entry-from-orbit condition.

Together, the periapsis raise and deorbit maneuvers have the potential of being expensive and merit an effort to minimize the total ΔV. The postaerocapture semimajor axis and the relative orientation of the deorbit and parking orbits may be varied such that the sum of parking orbit insertion and deorbit burns is minimized. In this minimization problem, the postaerocapture orbit is constrained to an initial periapsis radius no higher than 3440 km since this is the largest practical periapsis that results in an aerocapture maneuver. From the postaerocapture orbit, a periapsis raise maneuver is performed such that the parking orbit periapsis is sufficiently high (the parking orbit periapsis is constrained to no lower than 3780 km to maintain a safe 400-km periapsis altitude).

Three parameters (postaerocapture periapsis, postaerocapture semimajor axis, and parking orbit periapsis) are varied to determine the minimum total ΔV attainable. Note that a fourth parameter, the relative argument of periapsis between the parking orbit and deorbit orbit, is also internally varied to yield a minimum ΔV for any combination of the three other parameters. In general, it is observed that the minimum ΔV occurs at the highest attainable postaerocapture orbit periapsis radius and the lowest possible

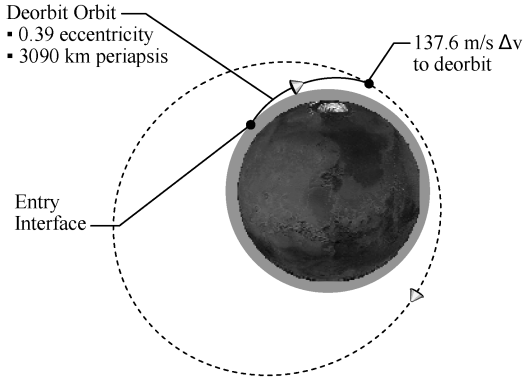

Fig. 5 Orbital maneuvers: deorbit and entry.

parking orbit periapsis radius. With the periapsis radii variables effectively driven to their prespecified bounds, the only variable remaining is postaerocapture orbit semimajor axis, which effectively controls the eccentricity of the postaerocapture orbit. Because an input into this orbit design process is the atmospheric entry state, a local minimum ΔV may be found which corresponds to the point where just enough orbital energy is removed from the vehicle during aerocapture.

Overall, this optimization results in a 63.8 m/s ΔV to raise periapsis and enter a parking orbit with an eccentricity of 0.30 and a 137.6 m/s ΔV to initiate the deorbit maneuver. With the application of a 25% ΔV margin, the resulting ΔV required for all maneuvers following aerocapture and preceding entry is found to be 251.8 m/s. Note that the ΔV margin of 25% is applied to address the uncertainties expected in the postaerocapture orbit. A 25% ΔV margin allows the system to accommodate a postaerocapture apoapsis radius between 6860 and 7520 km (the target apoapsis radius is 6980 km).

The deorbit maneuver targets an entry-from-orbit velocity of 4 km/s and inertial flight-path angle of −14.5 deg. For these conditions, the entry corridor is based on both the lift-down trajectory and the lift-up trajectory with the steepest flight-path angle having a peak deceleration of 5 g. As in the case of aerocapture, the 5-g limit is considered the maximum deceleration that a deconditioned human crew can tolerate for short durations [7,11]. The flight-path angle range between the lift-down and lift-up trajectory angles provides a navigable entry corridor. Entry and descent trajectories are simulated using POST [13].

C. Descent

Two types of terminal descent sequences were investigated: one that uses parachutes and one that does not. When using a parachute, the vehicle deploys a 30-m diam disk-gap-band (DGB) parachute at Mach 3, a significant extension over the 16-m, Mach 2 systems used in current robotic missions. A DGB parachute is chosen due to its proven performance at supersonic velocities in low density environments. The parachute is not allowed to grow beyond 30 m due to performance and fabrication concerns [2]. Additionally, the parachute is not permitted to begin deployment before Mach 3 due to aeroheating and area oscillation concerns in regimes above Mach 2 (deployment and inflation tests have been successfully performed up to about Mach 2.7 [14]). Descent scenarios that do not employ a parachute system make up the difference in deceleration through propulsion during the powered descent phase.

To estimate propellant and propulsion system mass requirements, analyses are performed by numerically integrating the nonlinear equations of motion with a gravity-turn control law. This control law was originally developed for the 1966–1968 lunar Surveyor landings and specifies that a spacecraft's thrust vector is maintained in the orientation opposite its velocity vector. Typically, the termination of a gravity turn is when the nadir angle, atmospheric relative velocity, and altitude above ground level are all zero. Here, the nadir angle is taken to be the angle subtended by the velocity vector and the gravitational acceleration vector. For the purposes of this study, two-dimensional gravity-turn trajectories are assumed to occur over a flat Mars and the gravity turn is designed to terminate at 50 m above ground level (AGL). The vehicle thrust is also assumed to be constant.

From a propellant mass perspective, it is desirable to begin the gravity-turn burn as late as possible, which allows maximum aerodynamic deceleration and minimizes gravity loss. However, if the burn begins too late, thrust requirements become unreasonably large. Previous studies [9] indicate that a thrust level of around 1.0 MN (approximately half the thrust of a space shuttle main engine) encompasses most reasonable cases of interest. For the cases investigated in this study, the required vehicle thrust-to-weight ratio on Earth (T/W_E) is in the range of 0.8 to 1.8.

A procedure is implemented to minimize vehicle mass (minimizing the sum of the propellant mass and propulsion system mass) by altering the time at which the gravity turn is initiated. None of the feasible cases investigated exhibit peak decelerations above 3.8 Earth g's. Note that the resulting propellant mass fraction is likely insufficient to satisfy pinpoint landing requirements associated with surface rendezvous mission architectures in which the crew system is required to land beside predeployed cargo assets. Such systems would require additional propellant over that obtained with the gravity-turn control law employed in this investigation.

D. Landing

A hover and cross-range capability is built into the powered descent profile, allowing for a modest degree of final maneuvering and hazard avoidance before landing. The maneuver assumes a cross-range requirement of 500 m at a 50-m altitude and provides a conservative estimate of ΔV and propellant requirements. This maneuver consists of three parts: cross-range acceleration, cross-range deceleration, and vertical descent. The required ΔV for this cross-range maneuver is approximately 265 m/s.

III. Modeling and Simulation

A. Design Atmosphere

The atmospheric density on Mars is highly dynamic due to changes in season, dust content, latitude, and time of day. Because of the significant variability in density that may be experienced, a statistically conservative atmosphere was developed using a Monte Carlo analysis of 1000 randomly generated atmospheric profiles. Each of these atmospheric profiles was generated using Mars-GRAM 2005 [15]. Among the 1000 profiles generated, the profile characterized by the 30-centile 0-km MOLA density point on a cumulative distribution function was selected. The entire atmospheric profile is retained to ensure that the atmospheric profile is consistent within itself and to ensure that hydrostatic equilibrium is satisfied. Note that by taking the profile with the 30% surface density atmosphere, 70% of the atmospheric density profiles simulated had a higher surface density and additional performance margin. This procedure yields a conservative yet realistic atmospheric profile relative to seasonal and diurnal cycles on Mars. The resulting density profile gives a 0-km MOLA density of 0.0124 kg/m^3.

B. Subsystem Sizing

1. *Heat-Shield Sizing*

Many human Mars EDL challenges center around heat-shield design. Several heat-shield material options were investigated, including the use of 1) phenolic impregnated carbon ablators (PICA) [16], used by the Stardust entry vehicle and potentially planned for use by the NASA Orion crew exploration vehicle, and 2) a carbon–carbon over FiberForm® system [17–19], similar to the Genesis heat-shield configuration. In each case, a single dual-use heat shield is found to provide better performance than two heat shields sized independently for aerocapture and entry from orbit. This result is primarily a function of the significantly higher aerothermodynamic environment of aerocapture (>6 km/s entry velocity) relative to entry-from-orbit (<4 km/s entry velocity). It is recognized that fabrication limitations and launch vehicle fairing constraints will restrict the size of any heat shield or heat-shield segment. Current launch vehicle fairings can accommodate elements with diameters up to 5 m, while many proposed launch vehicles (such as the Ares V proposed by NASA's Constellation Program) could potentially support payloads with diameters up to 10 m. Manufacturing and ground-based test limitations are also expected to be constraints. Current capabilities for the fabrication of carbon–carbon components offer significant size advantages relative to that demonstrated for PICA tiles. For this reason, a carbon–carbon over FiberForm heat shield is assumed in this reference mission. Current capabilities allow for the production of carbon–carbon heat-shield elements up to 3.66 m in diameter, corresponding to the largest carbon–carbon TPS fabrication facility at Carbon-Carbon Advanced Technologies, Inc. This study assumes a modest advance in TPS fabrication capability allowing single carbon–carbon sections to reach 5 m in their largest dimension. Even at a 5-m size, these carbon–carbon sections must be paneled to cover the 10 and 15-m

diam vehicles studied, resulting in seams along the windward side of the vehicle. Graphical representation of a potential tiling option is shown in Fig. 6. Although these seams create clear implementation challenges, this issue is not considered insurmountable. The Orion vehicle, for example, has considered numerous paneled heat-shield concepts, including paneled PICA tiles as large as 1.0×0.3 m. Further, the technical solution to the TPS paneling problem is not expected to have significant mass penalties and, therefore, does not strongly influence the results of this study.

The specific details of how a large heat shield of segmented tiles is assembled is not addressed here; however, the solution chosen may have significant system-level implications. Not least among these implications is the strong connection between capsule diameter and launch vehicle design/selection. It is conceivable that a 10-m diam launch vehicle may exist in the future; however, a 15-m diam vehicle is much larger than anything currently planned. Therefore, assembly and launch of large diameter vehicles is an area of technology development that may require significant investigation before human missions to Mars. Technology alternatives for large diameter aeroshells include on-orbit assembly and deployable/inflatable structures, although such endeavors will likely introduce additional technology challenges. Alternative configurations (including slender body aeroshells) better suited for launch vehicle integration should also be assessed. Certification, structural attachment, and development of a credible in-flight separation strategy are additional issues that require study.

After entry, the heat shield may need to allow for deployment of a parachute or inflatable aerodynamic decelerator (IAD) at supersonic speeds, and must allow for exposure of the descent engines. At least two propulsive reconfiguration options are possible: 1) the vehicle may drop the heat shield before engine ignition, or 2) doors may be opened in the heat shield to expose the engines. Significant challenges are encountered in both of these options. In the first option, the ballistic coefficient of the vehicle is generally greater than that of the heat shield (even with a 30-m DGB parachute deployed). Unless the ballistic coefficient of the heat shield is significantly greater than that of the remainder of the vehicle, it will not separate from the vehicle and there is risk of recontact between the heat shield and the vehicle/parachute. The second option (doors in the heat shield to expose engines) requires additional seams and/or penetrations in the heat shield, adding complexity and potential failure modes.

Other options that were considered but dismissed due to complexity or risk include the following: 1) Use of an exposed plug nozzle (e.g., aerospike engine) instead of a conventional bell nozzle [20]. This option requires a substantial amount of technology development. 2) Engines that deploy off the side or top of the vehicle. This is seen as complicated with many potential failure modes. 3) Engines facing toward the leeward side of the vehicle (engine bells at or near the apex of the cone). This would require the crew to experience a 180 deg rotation during the EDL sequence, creating unacceptable crew acceleration conditions (i.e., the deceleration during entry may be eyeballs in, resulting in eyeballs-out deceleration during powered descent). Despite the challenges associated with separating the heat shield, this traditional approach was chosen due to mass benefits, heat soak concerns, and operational heritage.

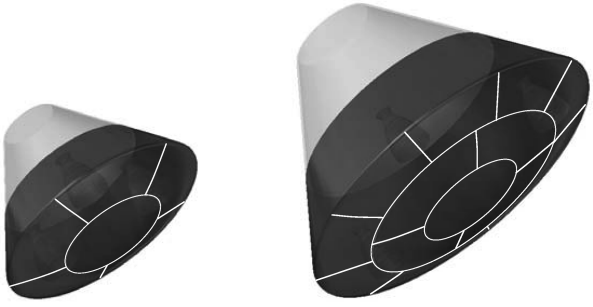

a) 10-m diam vehicle **b) 15-m diam vehicle**

Fig. 6 Possible carbon–carbon tile configuration on capsule vehicle.

Heat-shield mass estimation consists of two distinct segments. The first involves calculating the mass of the TPS and insulation material required to protect the vehicle during Mars aerocapture and entry, while the second provides a mass estimate of the underlying structure.

The carbon–carbon over FiberForm TPS analyzed in this study experiences no recession over the temperatures observed during Mars aerocapture or entry from orbit for any of the cases investigated. In determining the TPS mass, the carbon–carbon thickness is fixed at 1 mm (density of 1890 $\mathrm{kg/m^3}$) and the thickness of the FiberForm insulation (density of 180 $\mathrm{kg/m^3}$) is sized such that the temperature at the bond line remains below 250°C at all times. This maximum temperature is selected due to limitations of the bond-line adhesive. Further, because the capsule shapes considered in this study are flown at relatively high angles of attack, peak heating is expected not at the stagnation point, but along the leeward side, approaching the vehicle's shoulder. Based on the results of previous studies [21–23] on the aerothermodynamic heating experienced by blunt bodies at an angle of attack, the effect of increasing the shoulder heat rate by 15 to 150% (1.15 to 2.5x) of that seen at the stagnation point is investigated. From these data, the TPS mass is estimated by calculating the required TPS thickness and insulation thickness using a finite difference heat transfer calculation [24]. The results are shown in Table 2. Although the change in insulation thickness may be significant in some cases, the resulting mass penalty is relatively small. Therefore, while the effect of increased heat rate along the body is of critical importance in heat-shield design, the influence of such effects from a vehicle mass-sizing standpoint is fairly benign.

Finally, the underlying heat-shield structure is estimated as 10 or 15% of the total entry mass for the 10 or 15-m diam vehicles, respectively. The mass fraction is higher for the 15-m diam capsule because, given the same entry mass, the structure in a larger vehicle comprises a larger portion on the vehicle's mass. The magnitudes of these mass percentages are derived from the extrapolation of trends exhibited by historical capsule-shaped vehicles that jettisoned their heat shields before landing [2,25–27]. The underlying heat-shield structure in these missions is assumed to follow different trends than seen in missions where the heat-shield's structural support may be incorporated directly into the vehicle's primary structure.

2. *Parachute System Sizing*

A DGB parachute is selected for its proven performance at Mars. Because of the extremely heavy payload masses and the desire to maximize aerodynamic deceleration, all of the cases investigated in this study tended toward the 30-m diam limit previously discussed.

A parachute sizing tool developed for this study is used to estimate parachute mass. Canopy, suspension line, and riser masses are estimated based on material selection, parachute size, and vehicle mass [28]. Because of the high vehicle mass relative to parachute size, an infinite mass inflation [28] was assumed with peak loads occurring at full inflation. These expected loads are estimated using Pflanz's method with C_k values derived from historical DGB data [29]. Here, C_k is the opening load factor and may be used to find the peak load experienced at full inflation:

$$\text{peak load} = C_k q C_D A \tag{1}$$

Table 2 Effect of increased heat rate on TPS thickness and heat-shield mass

Peak heating scale factor	Increase in required insulation thickness	Increase in heat-shield mass
15% (1.15x)	4.5–17.5%	0.3–2.6%
30% (1.3x)	8.4–30.8%	0.6–4.6%
50% (1.5x)	12.9–45.8%	0.9–6.9%
100% (2.0x)	21.0–77.5%	1.4–11.7%
150% (2.5x)	26.5–100.8%	1.7–15.2%

Table 3 Structural mass fraction for selected crewed vehicles

Vehicle	Structural mass fraction (as % of dry mass)
Mercury [31]	15.2%
Gemini [31]	25.8%
Apollo CM [31]	19.2%
ESAS CEV[a] [32]	23.5%
DRM 3.0[a] [3]	24.7%

[a]Conceptual vehicle.

Here, q is dynamic pressure at parachute deployment conditions, C_D is the steady-state parachute drag coefficient, and A is the parachute reference area. Next, the masses of suspension lines, risers, and tapes are sized to withstand the maximum expected load with a factor of safety of 1.5. Further, the canopy mass is sized based on parachute diameter, opening loads, and the maximum expected dynamic pressure. Finally, the mortar mass is estimated based on historical mortar data. A simple regression analysis shows that the mortar mass may be estimated by the following expression, where m_m is the mortar mass (kg) and m_p is the parachute mass (kg) [30]:

$$m_m = 1.48 m_p^{0.5} \tag{2}$$

3. Backshell and Structure

Experience with crewed capsule-type vehicles (e.g., Apollo) as well as human Mars architecture studies (e.g., NASA's Mars DRM 3.0 [3]) suggests that mass, volume, and complexity benefits may be gained through the use of a backshell that is integral with the primary structure. Such a design is employed in this study. Historical data, summarized in Table 3, suggest that the structural mass fraction for a capsule-shaped vehicle with a combined backshell and primary vehicle structure is typically between 0.20–0.25. Therefore, in this study, the mass of the backshell and structure is conservatively estimated as 25% of the vehicle dry mass.

4. Propulsion System Sizing

Engine configuration presents a number of interesting challenges. First, an engine configuration trade is performed which investigates the use of one large engine or multiples of smaller engines. Figure 7 provides an example result from this analysis for the 15-m diam vehicle. The number of engines may be increased to an arbitrarily large number; however, the addition of more engines must always be balanced with increased complexity, risk, and cost. To mitigate these concerns, engine clusters consisting of more than four engines are not considered in this study.

The configuration with the largest number of engines placed around the periphery of the vehicle is found to be the best option from a performance standpoint for a number of reasons. First, numerous studies [33–36] have indicated that the interaction of the exhaust from forward facing engines with the oncoming flow at supersonic–hypersonic freestream velocities can have significant effects on the vehicle aerodynamic characteristics. Results indicate that the supersonic ignition of a single forward facing engine located in the center of the aeroshell can alter the bow shock and severely reduce (and in some cases nearly eliminate) the capsule's aerodynamic drag. It has been shown, however, that if the forward facing engines are placed near the periphery of the body, a significant portion of the vehicle's aerodynamic drag may be preserved during propulsive deceleration [33,34]. Second, a review of Fig. 7 shows that the four-engine option creates the largest amount of useful volume for the payload and propellant tanks while allowing ample space for access to the vehicle's outer wall. Space near the outer wall is required in both crew and cargo vehicles to allow room for hatches and windows. Finally, the four-engine configuration could also allow for an engine-out capability if each engine has sufficient gimbaling authority.

The propulsion system used during the powered flight portion of the EDL sequence is assumed to employ a liquid bipropellant engine using methane (CH_4, density of 422.6 kg/m^3) and liquid oxygen (LOX, density of 1140.1 kg/m^3) to remain consistent with the majority of previous human Mars exploration studies [3,10,37,38]. Although it is still in the development stage, this propellant combination is advantageous for Mars surface and ascent segments because of the relative ease by which carbon dioxide in the Martian atmosphere may be converted to methane through the Sabatier reaction ($CO_2 + 4H_2 \rightarrow CH_4 + 2H_2O$). The methane produced on Mars through this process may be used as propellant for the crew's ascent vehicle or other surface devices (such as LOX/CH4 fuel cells). For maximum commonality with the ascent vehicle, it is desirable to use the same propellant (or even engines) on both the descent vehicle and ascent vehicle. Finally, it is assumed that the LOX/CH4 engine used on this vehicle has an I_{sp} of 350 s at a mixture ratio of 3.5.

The propulsion system sizing algorithm assumes a scalable engine with a mass dictated by the following relationship:

$$m_{\text{engine}} = 0.00144T + 49.6 \tag{3}$$

where T is the engine thrust in Newtons and m_{engine} is the engine mass in kg. This expression is the result of a simple regression analysis performed on thrust vs mass data for a number of conceptual LOX/CH4 engines [39]. Note that this equates to an average engine thrust-to-weight ratio (on Earth) of about 67 for the vehicles investigated in this study. The maximum required thrust level was obtained from the results of the gravity-turn control law used during descent as well as the hover and cross-range maneuvers used during landing. Propellant tanks are assumed to be made of titanium and have an operating pressure of approximately 1.4 MPa (burst pressure of ~2.8 MPa).

Fig. 7 Engine configuration options for 15-m diam vehicle.

5. Reaction Control System Sizing

The reaction control system (RCS) provides orbital maintenance and vehicle orientation capability. The 12 thruster configuration used is based on the configuration employed by the Apollo command module. A hypergolic RCS system, using monomethyl hydrazine (MMH, density of 878 kg/m^3) [40] and nitrogen tetroxide (N_2O_4, density of 1440 kg/m^3) [40], is chosen for historical reasons—most RCS systems designed to date have relied on hypergolic propellants for simplicity and reliability. Each individual thruster is assumed to have a mass of 3.8 kg, operate at a mixture ratio of 2.16, and have an I_{sp} of approximately 289 s. The propellant tanks are sized in a fashion similar to that of the main propulsion system.

6. Command, Control, and Communications

Communication with the vehicle will be required during transit to Mars, during the time between aerocapture and entry, and after entry. It was estimated that the data rates required to fulfill mission needs will be on the order of tens of kbps, although the required data rate may be highly variable. For the crewed version of this vehicle, a higher data rate may be required (video transmissions may require data rates up to tens of Mbps [41]), although the high bandwidth communication required for this mission would be book kept separately under the human-specific payload. The baseline communications will consist of a 100 kbps X-band link (8 GHz) that will use the deep space network (DSN). From a mass-sizing standpoint, it is assumed that the vehicle will carry two amplifiers, two transponders, one primary high-gain antenna, and two smaller low-gain antennas.

7. Power

Power is provided by an outside source (service module or cruise stage-type device) during the transit from Earth to Mars. Once in the Mars vicinity, the vehicle must separate from the service module to prepare for aerocapture. From this point forward, the vehicle must provide power to run critical systems and support the payload. LOX/LH2 fuel cells are used to provide power for up to 72 h after separation from the service module to allow time for aerocapture, on-orbit checkout, and landing site phasing (LOX/CH4 fuel cells are also worth investigating if methane remains a top fuel choice for the descent or ascent vehicle). The LOX/LH2 fuel cells are assumed to consume 0.34 kg of O_2 and 0.05 kg of H_2 while producing 0.39 kg of H_2O for every kWh of energy produced. Additionally, assuming shuttle-class fuel cells, each fuel-cell unit has a mass of 91 kg and is capable of producing approximately 4.7 kW (peak of 12 kW) [42]. To support a human crew or a large payload, it is assumed that the vehicle is capable of supplying approximately 9 kW of electrical power [32].

In the event of a mission contingency in which a longer loiter time is needed than the fuel cells can provide (e.g., if a dust storm prohibits landing when the crew arrives), the crew must perform an orbital rendezvous with a prepositioned return vehicle to obtain power and consumables until they are able to descend to the surface. The crew vehicle could also be sized to accommodate an on-orbit loiter time longer than 72 h; however, the mass and volume of fuel-cell reactants increases significantly as the duration moves beyond a few days. For example, the fuel-cell system mass grows from 502 kg (0.2 m^3 of LOX and 0.5 m^3 of LH2) for a 72 h system to 1675 kg (1.0 m^3 of LOX and 2.1 m^3 of LH2) for a 14 day system. Other power solutions (e.g., solar arrays) were considered; however, such a system would require reconfiguration after aerocapture, increasing complexity. For example, if multijunction GaInP/GaAs solar arrays are used (efficiency of 108 W/m^2 at Mars) [43] to provide 9 kW of power, a large array size (approximately 83 m^2) would be required.

Before entry from orbit, the fuel cells are shut down and power will be drawn from a bank of lithium-ion batteries for a period of approximately 12 h. This provides sufficient time for entry, descent, and landing followed by initialization of (or connection to) the surface power source. The lithium-ion batteries are assumed to have an energy density of 0.15 kWh/kg.

8. Landing Hardware

Landing hardware will be required for the vehicle to make a soft touchdown on the Martian surface. Because this vehicle will carry the crew and other potentially sensitive payloads, landing gear is chosen over other options such as airbags or crushable material. Further, cargo unloading on the Martian surface creates the additional challenge of unloading cargo from a high platform above the surface. Because of the size of the landing system, engines, and propellant tanks, it is unlikely that the cargo will be very close to the Martian surface. For the purposes of this study, the landing gear mass is approximated as 3% of the vehicle landed mass [44].

9. Dry Mass Margin

Given the parametric nature of the designs presented in this study, all subsystem mass estimates are preliminary and significant uncertainty exists in the quantification of subsystem mass. As a result, a mass margin of 30% is applied to vehicle dry mass.

C. Sizing Algorithm Validation

The final step before assessing these human-class EDL systems is the validation of the mass-sizing tools. The output of the parachute sizing model is validated against three known cases where a DGB parachute was used on Mars: Viking, Mars Pathfinder (MPF), and the Mars Exploration Rovers (MER). As shown in Table 4, the model shows excellent correlation with known data points. The MER and MPF parachute mass data (supplied by Pioneer Aerospace Corporation) are split into two categories: 1) the parachute decelerator system and 2) the mortar deployer system. The parachute decelerator system is assumed to include all textile components except the bridle assembly and a titanium link. The mortar deployer system includes the bridle assembly and all mortar components, including the cover, sabot, pins/fasteners, tube, and ordnance.

Additionally, validation of other subsystem sizing algorithms and the entire simulation environment was performed through comparison with a Mars Science Laboratory (MSL)-class vehicle [46]. The mission sequence assumed in this comparison begins with a lifting hypersonic entry (initial conditions of 6 km/s at a radial distance of 3522 km and an inertial flight-path angle of −15.2 deg) [2], followed by descent on a supersonic DGB parachute. As the vehicle slows, the heat shield is dropped. At the mass-optimal point on the descent trajectory, propulsive descent is initiated and the backshell and parachute are separated. Once near the surface, the descent vehicle hovers for approximately 10 s while the rover is lowered to the surface on cables and then flies away.

Given that an MSL-class vehicle has an entry mass of about 3.2 t and a diameter of 4.6 m, only some of the tools may be realistically applied. Tools that remain relevant are the trajectory/gravity-turn analysis codes, heat-shield sizer, parachute sizer, backshell sizer,

Table 4 Validation of parachute sizing model

	Historical data				
	Parachute decelerator system, kg	Mortar deployer system, kg	Total mass, kg	Total calculated mass, kg	Error
Viking [30,45]	47	12	59	58.1	−1.53%
MPF	9.75	7.58	17.33	16.6	−4.21%
MER	16.46	7.55	24.01	26.8	11.62%

Table 5 Summary of EDL sizing tool validation—comparison for MSL-class vehicle

Parameter	MSL [46]	Validation for MSL-class vehicle
Aeroshell shape	70-deg sphere cone	Apollo capsule
Aeroshell diameter	4.6 m	4.6 m
Hypersonic L/D	0.22	0.22
Trajectory type	Guided (Apollo derived)	Lift-up boundary
TPS material	SLA-561	SLA-561
Supersonic parachute deployment (Mach no.)	2.0	2.0
Maximum total thrust during descent	18.3 kN	20.9 kN
Entry mass	3200 kg	3200 kg
Propellant mass	330 kg	340 kg
Landed payload	825 kg	840 kg
Payload mass fraction	25.8%	26.2%

propulsion system sizer, and dry mass margin. Other subsystems require substantially different models for an MSL-class vehicle (e.g., LOX/LH2 fuel cells do not make sense in this case) and are handled through mass fractions. When EDL system sizing is performed under these conditions, the results are as shown in Table 5. The agreement demonstrated on this validation problem is more than sufficient for conceptual design, as can be seen through the approximately 26% payload mass fraction.

IV. Summary of Mass-Sizing Results

Using the EDL system sizing tools developed for this study, a trade study is performed to investigate EDL system performance over a range of vehicle masses and diameters. Recall that a summary of the variables traded and the options considered is shown in Table 1.

An intuitive way to view the performance of each case is by payload mass fraction. These data are shown in Figs. 8 and 9. Note that vehicles with arrival masses between 40 and 80 t deliver surface payloads on the order of 15 to 30% of the arrival mass. Additionally, note that the 10-m diam aeroshell curves in Figs. 8 and 9 end before reaching an arrival mass of 100 t. The data points not plotted represent cases where insufficient aerodynamic deceleration causes the gravity turn to begin unrealistically early to meet the established thrust and acceleration limits. In these cases, the burn time is long and the propellant lost due to gravity effects is substantial. The large increase in required propellant mass results in a negative payload mass, a clearly infeasible result.

As expected, the cases that make use of a parachute show slightly better performance at lower masses, but the benefits gained become less pronounced as vehicle mass increases. For larger arrival masses, where parachute deployment occurs at a higher dynamic pressure, the mass of the parachute increases due to larger loads during

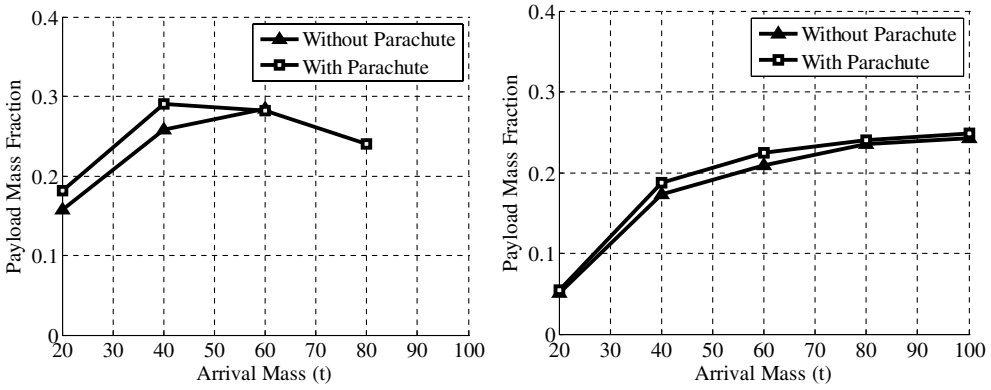

a) 10-m diam vehicle **b) 15-m diam vehicle**

Fig. 8 Payload delivered to the Martian surface as percentage of arrival mass for $L/D = 0.3$.

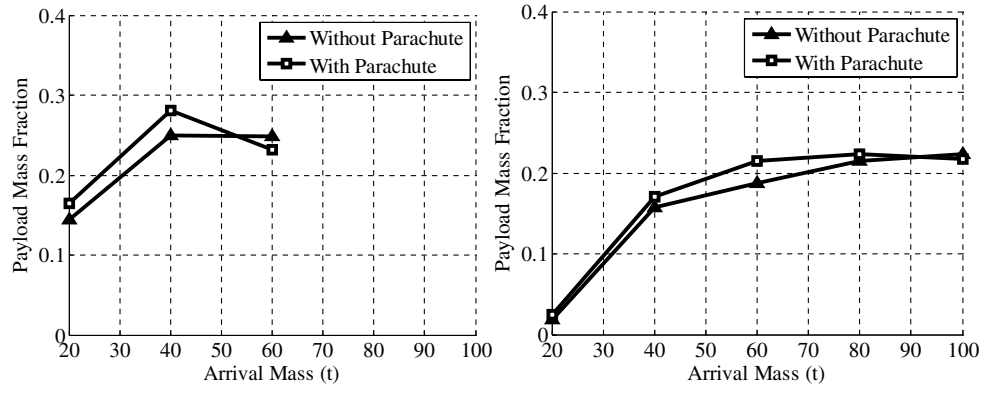

a) 10-m diam vehicle **b) 15-m diam vehicle**

Fig. 9 Payload delivered to the Martian surface as percentage of arrival mass for $L/D = 0.5$.

parachute deployment and inflation. Further, as the vehicle mass increases, the deceleration imparted by a 30-m diam parachute decreases. In all the cases investigated, the maximum payload mass benefit gained by using a 30-m parachute is 1.6 t.

At low arrival masses, the payload mass fraction is forced lower due to the significant impact of EDL system components with a fixed mass (e.g., power, communications, etc.). As arrival mass increases, the percentage of the arrival mass occupied by these systems decreases and the payload mass fraction increases. As arrival mass continues to increase, the ballistic coefficient becomes larger (for the fixed diameter aeroshell cases illustrated in these figures) and the vehicle experiences less aerodynamic deceleration. This pushes the burden of deceleration to the propulsion system and results in a decreasing payload mass fraction.

Comparing the results of the $L/D = 0.3$ and $L/D = 0.5$ cases, it is observed that the cases with the lower L/D can land slightly larger payloads on the Martian surface. The $L/D = 0.5$ cases, when flown on the lift-up entry profile bound, lead to faster trajectories because of reduced drag. This decreased aerodynamic deceleration places an increased burden on the descent propulsion system by causing the optimal point for gravity-turn initiation to occur at a higher velocity. Starting the gravity-turn at higher velocities requires more propellant, leading to a lower landed payload mass. This illustrates the importance of drag force for deceleration in the Martian atmosphere. It is important to note, however, that the best performance is typically not achieved through simply flying a ballistic entry to maximize C_D. Instead, optimal performance lies at a moderate L/D that provides sufficient drag for aerodynamic deceleration while also providing lift to extend the EDL time line.

The environmental control and life support system (ECLSS) required to support a crew of six for 3 days has a mass of approximately 2 t. Carrying the crew members themselves will require an additional metric ton. Therefore, it is estimated that in the limit, a crew capsule used only for descent could have an arrival mass as low as 20 t (the 10-m diam vehicles shown in Figs. 8 and 9 produce a payload mass fraction of about 0.15 for a 20 t vehicle or a surface payload of about 3 t). Other payloads, such as the ~20 t surface power system proposed in the Exploration Systems Architecture Study (ESAS) [32], would require a vehicle with an arrival mass on the order of 80 t. Note that a larger diameter vehicle may be required to land payloads of this mass. In addition, no feasible cases were obtained with the capability to deliver more than approximately 25 t of payload to the Mars surface for arrival masses less than 100 t.

To provide insight into the individual subsystem contributions to the overall vehicle mass, an example mass breakdown is shown in Table 6 for the 10-m diam, 40-t vehicle that is flown at an L/D of 0.3. Similar subsystem mass breakdowns result across the range of feasible vehicles analyzed in this investigation.

Table 6 Mass breakdown for 10-m diam, 40-t vehicle with no parachute and $L/D = 0.3$

Subsystem/component	Mass fraction, % of m_{arrival}
Heat shield	12.1%
Parachute and mortar	——
Backshell and structure	12.5%
Propulsion system	3.5%
Orbital maneuvering system (OMS) and RCS	0.5%
Command, control, and communication	1.1%
Power system	3.3%
Landing gear	1.9%
Margin	15.0%
OMS and RCS propellant	8.5%
Descent propellant	16.0%
Payload	25.5%

V. Comparison with Past Missions and Architecture Studies

A. Comparison of Mass, Size, and Volume

Many of the challenges seen in this investigation may be explained through a comparison of the ballistic coefficients of vehicles considered in this study with previous robotic [2] and crewed [31,32,47–50] missions (see Fig. 10). First, recall that ballistic coefficient β is given by

$$\beta = \frac{m}{C_D A} \tag{4}$$

From the data shown in Fig. 10, it is clear that the capsule shapes investigated in this study achieve a higher L/D through a reduction in drag. This is evident from the higher β (lower $C_D A$) associated with configurations flown at an L/D of 0.5 (as compared to those at an L/D of 0.3). High ballistic coefficients in conjunction with the thin Martian atmosphere contribute to the difficulties experienced in deploying parachutes or beginning propulsive descent at reasonable altitudes and velocities. The lack of aerodynamic drag relative to vehicle momentum results in a lower-altitude atmospheric deceleration and unfavorable conditions for the initiation of events that occur toward the end of the EDL time line. Comparing the ballistic coefficients produced by the parametric investigations of this study with previous or planned missions in Fig. 10, all planned Mars missions have a β below 120 kg/m^2 and all previous Earth crewed vehicles have a β below ~600 kg/m^2. Further, note the correlation between successful mass-diameter-L/D combinations (see Figs. 8 and 9) and ballistic coefficient (vehicle designs for Mars cease to converge as β exceeds about 900 kg/m).

It is also instructive to compare the packaging density of previous missions and those generated by the parametric investigations performed in this study (see Fig. 11). The first observation is that crewed vehicles have historically produced higher packaging densities than seen in robotic missions. Further, if the existing crewed mission data are extrapolated to the capsule sizes investigated in this study, it is clear that the cases deemed infeasible (a negative surface payload mass) in this study lie significantly outside the feasible packaging density trend suggested by historical data. These data suggest that a 10-m diam vehicle should have an arrival mass of less than about 60 t, while a 15-m diam vehicle could sustain an arrival mass over the entire 20–100-t range considered.

Expanding on the subject of volumetric constraints, given the four-engine configuration chosen, pressurized volumes will not be able to exceed approximately 59 and 322 m^3 in the 10 and 15-m diame vehicles, respectively. These pressurized volumes are compared to those achieved by past human-rated capsule vehicles in Table 7. Note the significant effect that the descent engines have on the amount of space within the capsule that is usable for payload (this effect is most evident in the 10-m diam vehicle). Further, a significant

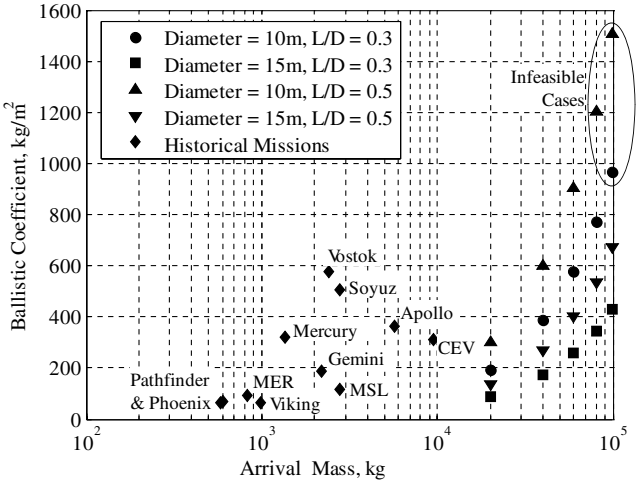

Fig. 10 Ballistic coefficient, β, trends as a function of mass.

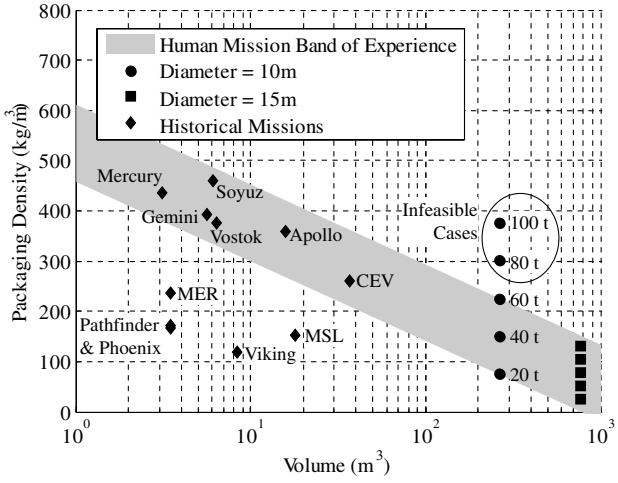

Fig. 11 Packaging density trends as a function of vehicle volume.

portion of this pressurized volume will be taken up by cargo, crew accommodations, and other subsystems, resulting in a habitable volume that is noticeably lower than the pressurized volume listed in Table 7.

Previous studies [51] and NASA standards [11] suggest that a six-person crew would require a habitable volume of no less than $\sim$60 m^3 (with optimal performance at habitable volumes greater than $\sim$120 m^3) for durations on the order of the transit time from Earth to Mars. Based on these criteria, the crew may need a separate habitat for the transit to and from Mars if the 10-m diam vehicle is chosen. Additionally, if the capsule were to be used as crew living quarters on the Martian surface, there is very limited floor space. Given the ceiling height required for humans to comfortably move about on the surface, even the 15-m diam capsule has only a usable floor area of $\sim$23 m^2. This underscores the need for a dedicated habitat for a human Mars mission. Unfortunately, a rigid habitat of sufficient size cannot be packaged in the capsule shape. To land a habitat on the Martian surface, one of two approaches would be necessary: 1) use of an inflatable habitat or 2) flight of a separate entry system for the habitat and other large payloads, coupled with a surface rendezvous.

B. Comparison of Payload Performance

From a direct comparison of payload performance, it is clear from Figs. 8 and 9 that the majority of reasonable scenarios yield a payload mass fraction between 15 and 30%. These payload mass fractions are consistent with the performance demonstrated by previous and planned robotic missions to Mars, as shown in Table 8.

Although the payload mass fractions observed in this study agree with past robotic missions, there are many differences between robotic and crewed missions that likely affect the payload mass fraction. These payload mass fractions, therefore, are also compared with two of the major human mars mission architectures developed to date: NASA's DRM 3.03 and Mars Direct [37,52]. The assumptions made and performance estimated in these architectures are compared to the results of this study in Table 9.

Among the most important conclusions from this comparison is that this study estimates a payload mass fraction that is 20–30% lower than what has been suggested by previous studies. The cause of this difference comes primarily from two sources: the dry mass margin included in this investigation and the reliance on parachutes that greatly exceeds known size and performance limitation in past studies. Note that the results presented in this study include a 30% dry mass margin on the EDL system that equates to 13.5 to 24.1% of the arrival mass, depending on the specific scenario. Margin alone, therefore, accounts for the majority of the difference between the 20–30% payload mass fraction seen in this study and the 50–60% reported in DRM 3.0 and Mars Direct.

The other major factor contributing to the difference in performance between various cases is the reliance on parachutes. Both DRM 3.0 and Mars Direct rely on parachutes to decelerate to subsonic conditions, the size and complexity of which would require major technology breakthroughs. By limiting the parachute to a diameter below 30 m and a deployment velocity below Mach 3 and using supersonic retropropulsion, this investigation requires more propellant to decelerate than these earlier studies (indicated by larger descent ΔV requirements). This causes a more massive propulsion system, primarily due to the larger tanks required for the increased propellant quantities.

VI. Conclusions

This study has explored, from a configuration and mass-sizing perspective, how traditional entry system technologies may be used for the human exploration of Mars. This analysis was enabled by the integration of trajectory and subsystem mass-sizing algorithms for human-class Mars missions. The results suggest that capsule-shaped vehicles with arrival masses in the 20—100-t range would be capable of deploying surface payloads with a mass on the order of 5–25 t. This is equivalent to surface payload masses that are only 15–30% of the arrival mass. Note that the payload mass fractions presented here are much lower than has been assumed in many human Mars mission

Table 7 Comparison of total capsule volume and pressurized volume for human-rated capsule vehicles

Vehicle	Total interior volume, m^3	Pressurized volume, m^3	Usable %
Mercury [31]	3.11	1.42	46%
Gemini [31]	5.61	2.27	40%
Apollo CM [31]	15.74	10.36	66%
Soyuz descent module [50]	6.1	3.85	63%
10-m diam capsule	266	59	26%
15-m diam capsule	764	322	42%

Table 8 Payload mass fractions for past successful and planned robotic Mars missions [2]

Mission	Landing year	Entry mass, kg	Surface payload mass, kg	Payload mass fraction
Viking 1 & 2	1976	992	244	24.6%
MPF	1997	584	92	15.8%
MER-A	2004	827	173	20.9%
MER-B	2004	832	173	20.8%
Phoenix (planned)	2008	600	167	27.8%
MSL (planned)	2010	3200	825	25.8%

Table 9 Comparison of EDL assumptions and performance between various human Mars architectures

Characteristics	Present investigation	DRM 3.0 [3]	Mars Direct [37,52]
Aerocapture	Yes	Yes	Yes
Vehicle outer mold line	Blunt-body (capsule) with $L/D = 0.3$ or 0.5	Triconic with $L/D = 0.6$	Deployable "umbrella shaped"
Heat shield	11.0–22.3% of entry mass	16–18% of entry mass	Unknown
Parachutes	Recommended: No. If yes, single 30-m diam DGB parachute deployed at Mach 3. Mass > 147 kg	Yes. Cluster of four 50-m diam DGB parachutes deployed at an altitude of 8 km and a velocity of 700 m/s (Mach 3.2). Mass = 700 kg	Yes. Unspecified size, type, and deployment conditions
Propulsive descent	Yes. LOX/CH4 engines with propulsion system mass: <3.7 t	Yes. LOX/CH4 engines with propulsion system mass: ~1.0 t	Yes. LOX/CH4 engines
Propulsive ΔV	735–1267 m/s	632 m/s	<700 m/s
Arrival mass	20–100 t	60.8–66.0 t	40.6–46.2 t
Surface payload mass	<25 t	30.9–40.2 t	25.2–28.6 t
Payload mass fraction	<29% (30% margin on EDL sys)	50.8–60.9% (no mass margin)	62% (no mass margin)

conceptual studies. None of the cases investigated in this study (constrained to an arrival mass below 100 t) are capable of landing a payload with a mass exceeding about 25 t. This may become a significant concern if human mission surface components (habitat, power system, In Situ Resource Utilization plant, rovers, etc.) cannot be separated into segments with sufficiently small masses. Future work should include incorporation of a detailed EDL design into Mars design reference missions to assess the system-level impacts. An additional challenge was shown to be habitable volume (during transit) and usable floor space (once landed on Mars). Because of its sloped sidewalls, payload volume restrictions are seen to be a major drawback of the capsule shape. Despite these drawbacks, the capsule shape is a promising configuration for delivering the crew to the Martian surface. Other aeroshell shapes (e.g., slender body configurations) should be investigated as they may provide more packaging flexibility for large payloads. However, care must be taken with slender body shapes so as to not sacrifice aerodynamic drag area and hence deceleration performance.

In summary, simply extending conventional technologies developed for robotic exploration is not likely sufficient to support human-class missions to the surface of Mars. Technology development in areas such as aerocapture, aeroshell configuration, supersonic propulsive deceleration, TPS paneling, and inflatable aerodynamic decelerators will likely be required to enable these missions.

Acknowledgments

The authors thank the following individuals for their help and insight in the preparation of this manuscript: Juan Cruz, John Dec, and Karl Edquist of the NASA Langley Research Center, Allen Witkowski of Pioneer Aerospace Corporation, James Thompson of Carbon-Carbon Advanced Technologies, Inc., Ashley Korzun and Charity Lewis of the Georgia Institute of Technology, and Kavya Manyapu of the Lockheed Martin Corporation. Their support is greatly appreciated.

References

[1] "Vision for Space Exploration," National Aeronautics and Space Administration, NASA NP-2004-01-334-HQ, Feb. 2004.

[2] Braun, R. D., and Manning, R. M., "Mars Entry, Descent, and Landing Challenges," *Journal of Spacecraft and Rockets*, Vol. 44, No. 2, 2007, pp. 310–323. doi:10.2514/1.25116

[3] Drake, B. G. (ed.), "Reference Mission Version 3.0, Addendum to the Human Exploration of Mars: The Reference Mission of the NASA Mars Exploration Study Team," NASA Johnson Space Center EX13-98-036, June 1998.

[4] Walberg, G. D., "A Survey of Aeroassisted Orbit Transfer," *Journal of Spacecraft and Rockets*, Vol. 22, No. 1, 1985, pp. 3–18.

[5] Hall, J. L., Noca, M. A., and Bailey, R. W., "Cost-Benefit Analysis of the Aerocapture Mission Set," *Journal of Spacecraft and Rockets*, Vol. 42, No. 2, 2005, pp. 309–320.

[6] Tartabini, P. V., Munk, M. M., and Powell, R. W., "Development and Evaluation of an Operational Aerobraking Strategy for Mars Odyssey," *Journal of Spacecraft and Rockets*, Vol. 42, No. 3, 2005, pp. 423–434.

[7] Lyne, J. E., "Physiologically Constrained Aerocapture for Manned Mars Missions," NASA TM-103954, Aug. 1992.

[8] Hofstetter, W. K., Wooster, P. D., Nadir, W. D., and Crawley, E. F., "Affordable Human Moon and Mars Exploration Through Hardware Commonality," *Space 2005*, AIAA Paper 2005-6757, Aug. 2005.

[9] Wells, G., Lafleur, J., Verges, A., Manyapu, K., Christian, J., Lewis, C., and Braun, R., "Entry, Descent and Landing Challenges of Human Mars Exploration," American Astronautical Society Paper 06-072, Feb. 2006.

[10] Griffin, B., Thomas, B., Vaughan, D., Drake, B., Johnson, L., and Woodcock, G., "A Comparison of Transportation Systems for Human Mission to Mars," AIAA Paper 2004-3834, July 2004.

[11] Man-Systems Integration Standards, Rev. B, NASA STD-3000, July 1995.

[12] Wooster, P. D., Braun, R. D., Ahn, J., and Putnam, Z. R., "Mission Design Options for Human Mars Missions," *MARS: The International Journal of Mars Science and Exploration*, Vol. 3, Aug. 2007, pp. 12–28.

[13] POST, Program to Optimize Simulated Trajectories, Ver. 5.2, NASA Langley Research Center, Hampton, VA, Martin Marietta Corporation, Denver, CO, 1997.

[14] Cruz, J. R., and Lingard, J. S., "Aerodynamic Decelerators for Planetary Exploration: Past, Present, and Future," AIAA Paper 2006-6792, Aug. 2006.

[15] Mars-GRAM, Mars Global Reference Atmospheric Model, Ver. 2005, Computer Sciences Corporation, Huntsville, AL, NASA Marshall Spaceflight Center, AL, 2005.

[16] Tran, H. K., Johnson, C. E., Rasky, D. J., Hui, F. C. L., Hsu, M., and Chen, Y. K., "Phenolic Impregnated Carbon Ablators (PICA) for Discovery Class Missions," AIAA Paper 1996-1911, June 1996.

[17] Selvaduray, G., and Cox, M., "1997-1998 Annual Report Thermal Protection Materials Development," NASA CR-1998-208331, 1998.

[18] Parmenter, K., Milstein, F., DiCarlo, A., Lotz, R., Mencher, J., Guerra, E., Luna, C., and Valenzuela, P., "Characterization of Lightweight Ceramic Ablator Materials," University of California, Santa Barbara, NASA Research Grants NAG 2-1148 and NCC 2-1049, 4 Feb. 1999.

[19] Tran, H., Rasky, D., and Esfahani, L., "Thermal Response and Ablation Characteristics of Lightweight Ceramic Ablators," *Journal of Spacecraft and Rockets*, Vol. 31, No. 6, 1994, pp. 993–998.

[20] Bono, P., "ROMBUS—An Integrated Systems Concept for a Reusable Orbital Module (Booster and Utility Shuttle)," AIAA Paper 1963-271, June 1963.

[21] Li, C. P., "Calculation of Convective Heat Transfer on Highly Blunt Bodies at Flow Incidence," AIAA Paper 1989-244, Jan. 1989.

[22] Edquist, K. T., and Alter, S. J., "Computational Aeroheating Predictions for Mars Lander Configurations," AIAA Paper 2003-3639, June 2003.

[23] Edquist, K. T., "Afterbody Heating Predictions for a Mars Science Laboratory Entry Vehicle," AIAA Paper 2005-4817, June 2005.

[24] Dec, J. A., and Braun, R. D., "An Approximate Ablative Thermal Protection System Sizing Tool for Entry System Design," AIAA Paper 2006-780, Jan. 2006.

[25] Ezell, E. C., and Ezell, L. N., *ON MARS, Exploration of the Red Planet 1958–1978*, SP-4212, NASA, 1984, pp. 447–452.

[26] Nolte, L. J., and Stephenson, D. S., "Final Report—System Design of the Pioneer Venus Spacecraft, Volume 5: Probe Vehicle Studies," NASA CR-137492, July 1973.

[27] Givens, J. J., Nolte, L. J., and Pochettino, L. R., "Galileo Atmospheric Entry Probe System: Design, Development and Test," AIAA Paper 1983-98, Jan. 1983.

[28] Kanacke, T. W., "Parachute Recovery Systems Design Manual," NWC

TP 6575, Para Publishing, 1992.
[29] Cruz, J. R., "Opening Loads Analyses for Various Disk-Gap-Band Parachutes," AIAA Paper 2003-2131, May 2003.
[30] Ewing, E. G., Bixby, H. W., and Knacke, T. W., *Recovery System Design Guide*, AFFDL-TR-78-151, 1978.
[31] Heineman, W., "Fundamental Techniques of Weight Estimating and Forecasting for Advanced Manned Spacecraft and Space Stations," NASA TN-D-6349, May 1971.
[32] "NASA's Exploration Systems Architecture Study," NASA TM-2005-214062, Nov. 2005.
[33] Jarvinen, F. O., and Adams, R. H., "The Effects of Retrorockets on the Aerodynamic Characteristics of Conical Aeroshell Planetary Entry Vehicles," AIAA Paper 1970-219, Jan. 1970.
[34] Keyes, J. W., and Hefner, J. N., "Effect of Forward-Facing Jets on Aerodynamic Characteristics of Blunt Configurations at Mach 6," *Journal of Spacecraft and Rockets*, Vol. 4, No. 4, 1967, pp. 533–534.
[35] Fomin, V. M., Maslov, A. A., Malmuth, N. D., Fomichev, V. P., Shashkin, A. P., Korotaeva, T. A., Shiplyuk, A. N., and Pozdnyakov, "Influence of a Counterflow Plasma Jet on Supersonic Blunt-Body Pressures," *AIAA Journal*, Vol. 40, No. 6, 2002, pp. 1170–1177.
[36] Daso, E. O., Pritchett, V. E., Wang, T., Ota, D. K., Blankson, I. M., and Auslender, A. H., "The Dynamics of Shock Dispersion and Interactions in Supersonic Freestreams with Counterflowing Jets," AIAA Paper 2007-1423, Jan. 2007.
[37] Zubrin, R. M., Baker, D. A., and Gwynne, O., "Mars Direct: A Simple, Robust, and Cost Effective Architecture for the Space Exploration Initiative," AIAA Paper 1991-0329, Jan. 1991.
[38] Christian, J., Tanner, C., and Theisinger, J., "A Revolutionary Outpost Architecture for Human Mars Exploration," International Astronautical Congress Paper IAC-06-D1.1.7, Oct. 2006.
[39] Klepikov, I. A., Katorgin, B. I., and Chvanov, V. K., "The New Generation of Rocket Engines, Operating by Ecologically Safe Propellant 'Liquid Oxygen and Liquefied Natural Gas (Methane)'," *Acta Astronautica*, Vol. 41, Nos. 4–10, 1997, pp. 209–217. doi:10.1016/S0094-5765(98)00076-9
[40] Humble, R.W., Henry, G. N., and Larson, W. J., *Space Propulsion Analysis and Design*, McGraw–Hill, New York, 1995, pp. 695–714.
[41] Comparetto, G. M., "Command, Control, and Communications Architecture," *Human Spaceflight Analysis and Design*, edited by W. J. Larson and L. K. Pranke, McGraw–Hill, New York, 1999, pp. 869–905.
[42] Landis, G. A., McKissock, B. I., and Bailey, S. G., "Designing Power Systems," *Human Spaceflight Analysis and Design*, edited by W. J. Larson and L. K. Pranke, McGraw–Hill, New York, 1999, pp. 656–658.
[43] McDermott, J. K., "Spacecraft Subsystems: Power," *Space Mission Analysis and Design*, 3rd ed., edited by J. R. Wertz and W. J. Larson, Kluwer Academic, Boston, MA, 1999, pp. 407–427.
[44] Hofstetter, W., de Weck, O., and Crawley, E., "Modular Building Blocks for Manned Spacecraft: A Case Study for Moon and Mars Landing Systems," *2005 International Council on Systems Engineering (INCOSE) International Symposium*, 2005.
[45] Witkowski, A., and Bruno, R., "Mars Exploration Rover Parachute Decelerator System Program Overview," AIAA Paper 2003-2100, May 2003.
[46] Striepe, S. A., Way, D. W., Dwyer, A. M., and Balaram, J., "Mars Science Laboratory Simulations for Entry, Descent, and Landing," *Journal of Spacecraft and Rockets*, Vol. 43, No. 2, 2006, pp. 311–323.
[47] Brown, S. W., and Moseley, W. C., "Summary of Wind-Tunnel Investigations of the Static Longitudinal Stability Characteristics of the Production Mercury Configurations at Mach Numbers from 0.05 to 20," NASA TM-X-491, Feb. 1961.
[48] Griffith, B. J., "Comparison of Aerodynamic Data from the Gemini Flights and AEDC-VKF Wind Tunnels," *Journal of Spacecraft and Rockets*, Vol. 4, No. 7, 1967, pp. 919–924.
[49] Johnson, N. L., *Handbook of Soviet Manned Space Flight*, American Astronautical Society Science and Technology Series, Vol. 48, Univelt, San Diego, CA, 1980.
[50] Hall, R. D., and Shayler, D. J., *Soyuz: A Universal Spacecraft*, Praxis Publishing, Chichester, U.K., 2003, pp. 39–74.
[51] Fraser, T. M., "The Effects of Confinement as a Factor in Manned Space Flight," NASA CR-511, 1966.
[52] Zubrin, R., *The Case for Mars*, Touchstone, New York, 1997, pp. 1–18, 75–112, 139–170.

C. Kluever
Associate Editor